SUPPORTING INFORMATION

Bioconcentration and Biotransformation of Amitriptyline in Gilt-head Bream

Haizea Ziarrusta*,[1,2] Leire Mijangos,[1] Urtzi Izagirre,[3] Merle M. Plassmann,[2] Jonathan P. Benskin,[2] Eneritz Anakabe,[4] Maitane Olivares,[1] Olatz Zuloaga,[1,3]

1. Department of Analytical Chemistry, University of the Basque Country (UPV/EHU), Leioa, Basque Country, Spain
2. Department of Environmental Science and Analytical Chemistry (ACES), Stockholm University, Stockholm, Sweden
3. Research Centre for Experimental Marine Biology and Biotechnology (PIE), University of the Basque Country (UPV/ EHU), Plentzia, Basque Country, Spain
4. Department of Organic Chemistry, University of the Basque Country (UPV/EHU), Leioa, Basque Country, Spain

*Corresponding author: Haizea Ziarrusta (haizea.ziarrusta@ehu.eus)

Department of Analytical Chemistry, Faculty of Science and Technology, University of the Basque Country (UPV/EHU), P.O. Box 644, 48080 Bilbao, Spain.

Tel: + 34 94 601 55 51; Fax: +34 94 601 35 00

The supporting data contains 18 pages, with 2 Tables and 4 Figures.

Reagents information

Methanol (MeOH, HPLC grade, 99.9 %) and acetone (HPLC grade, 99.8 %) were supplied by LabScan (Dublin, Ireland), acetonitrile (HPLC grade, 99.9 %) and ethyl 3-aminobenzoate methanesulfonate (tricaine, ≥ 98%) by Sigma–Aldrich (Steinheim, Germany), sodium hydroxide pellets (NaOH, ≥ 99 %) by Merck (Darmstadt, Germany), formic acid (HCOOH, ≥ 98 %) by Scharlau (Barcelona, Spain) and ammonium hydroxide (NH_4OH, 25 %), ethylenediaminetetraacetic acid (EDTA, ≥ 99 %) and sodium hydrogen carbonate ($NaHCO_3$, ≥ 99.9 %) by Panreac (Barcelona, Spain). Ultra-pure water was obtained using a Milli-Q water purification system (<0.05 S/cm, Milli-Q model 185, Millipore, Bedford, MA, USA). MeOH (Fisher Scientific, Loughborough, UK) was used as mobile phase solvent and formic acid (HCOOH, Optima, Fischer Scientific, Gell, Belgium) for mobile phase modifications.

High purity nitrogen gas (>99.999 %) supplied by Messer (Tarragona, Spain) was used as collision gas in liquid chromatography-triple quadrupole-tandem mass spectrometry (LC-QqQ-MS/MS) and for evaporation purposes in the Turbo Vap LV Evaporator (Zymark, Hopkinton, MA, USA). Nitrogen gas (99.999 %), provided by Air Liquide (Madrid, Spain), was used as both nebulizer and drying gas.

LC-QqQ-MS/MS analysis

Chromatographic separation was carried out using an Agilent 1260 series HPLC equipped with a Kinetex biphenyl 100 Å core-shell (2.1 mm x 50 mm, 2.6 μm) chromatographic column with a Kinetex biphenyl 100 Å core-shell pre-column (2.1 mm x 5 mm, 2.6 μm) from Phenomenex (Torrance, CA, USA). The mobile phases consisted of Milli-Q water:MeOH (95:5, v/v) mixture (A) and MeOH:Milli-Q water (95:5, v/v) mixture (B), both containing 0.1 % HCOOH. The eluent gradient profile started with 55 % B, which was increased to 90 % B by 3 min, maintained at isocratic conditions for 6 min, and then returned to initial conditions by 12 min. The column was subsequently equilibrated for 8 min (total run time = 20 min). The flow rate was maintained at 0.3 mL/min and the injection volume was 2 μL. The HPLC was coupled to an Agilent 6430 triple quadrupole (QqQ) mass spectrometer (Agilent Technologies, Palo Alto, CA, USA) via an electrospray ionization (ESI) source. The MS was operated in positive ionization selected reaction monitoring (SRM) mode. The capillary voltage was set at 3000 V, with a drying gas flow rate of 12 L/min, a nebulizer pressure of 45 psi and a drying gas temperature of 350 °C. AMI was quantified using the *m/z* 278.2/191.1 precursor-to-product ion transition, with *m/z* 278.2/117.1 and 278.2/91.1 as confirmation ions. NOR was quantified using *m/z* 264.2/233.1, and confirmed using *m/z* 264.2/105.1 and 264.2/91.1. Instrumental operations, data acquisition and peak integration were performed with the Masshunter Workstation Software (Qualitative Analysis, Version B.06.00, Agilent Technologies).

LC-q-Orbitrap analysis

The analysis was carried out using a Thermo Scientific Dionex UltiMate 3000 UHPLC coupled to a Thermo Scientific™ Q Exactive™ HF hybrid quadrupole-Orbitrap mass spectrometer equipped with a heated ESI source (Thermo, CA, USA). Extracts were separated on a Hypersil GOLD aQ (2.1 mm x 100 mm, 1.9 μm) chromatographic column with a prefilter (2.1 mm ID, 0.2 μm) from Thermo (CA, USA), using a mobile phase of Milli-Q water (solvent A) and ACN (solvent B), both containing 0.1 % HCOOH. The LC gradient started at 10 % B with a linear increase to 50 % B at 9 min and further to 95 % B at 12 min. After 1.5 min at 95 % B, the gradient was returned to initial conditions for 1.5 min. The flow rate was set to 0.4 mL/min at a column temperature of 35 °C. The injection volume was 5 μL and the autosampler was maintained at 5 °C.

The Orbitrap was operated in full scan – data dependant MS2 (Full MS-ddMS2) acquisition mode. One full scan at a resolution of 120 000 full width at half maximum (FWHM) at *m/z* 200 over a scan range of *m/z* 100-600 was followed by five ddMS2 scans at a resolution of 15 000 FWHM at *m/z* 200, with an isolation window of 0.4 Da. The normalized collision energy (NCE) in the higher-energy collisional dissociation (HCD) cell was set to 35 %. The ddMS2 scans were acquired on an inclusion list of ions that had been either described previously[20] or determined in a pre-run of 12 samples (one control and one exposed per matrix) where a full scan (resolution 120 000) was combined with an all ion fragmentation (resolution 60 000 and NCE 35 %). This resulted in an inclusion list of 108 ions in positive mode and 90 ions in negative mode. If no ions from the inclusion list were detected in the previous full scan, the most intense ions from the full scan were chosen for fragmentation. The ddMS2 scans were run with an intensity threshold of 2.7×10^4, a dynamic exclusion of 5 s and an apex trigger between 1 and 6 s. Total scan cycle time was ~0.4 s, based on a 256 ms high resolution scan and five, 32 ms ddMS2 scans. The HESI source parameters were set to 4.5 kV spray voltage, 350 °C capillary temperature, 45 arbitrary units (au) sheath gas (nitrogen), 5 au AUX gas and 300 °C AUX gas heater. External calibration of the instrument was conducted immediately prior to analysis using Pierce LTQ ESI Calibration Solutions (Thermo Scientific, Waltham, Massachusetts, United States). The instrument was controlled by Xcalibur 3.1 (Thermo).

Table S1: Phase I and Phase II reactions that Compound Discoverer takes into account to predict possible metabolites of AMI.

Phase I reactions	
Dehydration	H_2O ->
Desaturation	H_2 ->
Hydration	-> H_2O
Nitro Reduction	O_2 -> H_2
Oxidation	-> O
Oxidative Deamination to Alcohol	H_2N -> HO
Oxidative Deamination to Ketone	H_3N -> O
Reduction	-> H_2
Thiourea to Urea	S -> O
Phase II reactions	
Acetylation	H -> C_2H_3O
Arginine Conjugation	H O -> $C_6H_{13}N_4O_2$
Glucoside Conjugation	H -> $C_6H_{11}O_5$
Glucuronide Conjugation	H -> $C_6H_9O_6$
Glutamine Conjugation	HO -> $C_5H_9N_2O_3$
Glycine Conjugation	HO -> $C_2H_4NO_2$
GSH Conjugation 1	-> $C_{10}H_{15}N_3O_6S$
GSH Conjugation 2	-> $C_{10}H_{17}N_3O_6S$
Methylation	H -> CH_3
Ornithine Conjugation	HO -> $C_5H_{11}N_2O_2$
Palmitoyl Conjugation	H -> $C_{16}H_{31}O$
Stearyl Conjugation	H -> $C_{18}H_{35}O$
Sulfation	H -> HO_3S
Taurine Conjugation	HO -> $C_2H_6NO_3S$

Table S2: Molecular formula, theoretical m/z of $[M+H]^+$ and the corresponding ΔMass (ppm) for each tissue, the most abundant fragments in the MS2 spectra and the retention time for AMI and all annotated metabolites.

Compound	Molecular Formula (M)	Theoretical m/z ($[M+H]^+$)	Fragments in MS2 spectra	ΔMass (ppm)						R_t (min)
				Liver	Plasma	Bile	Brain	Muscle	Gill	
AMI	$C_{20}H_{23}N$	278.19028	278.18988, 233.13226, 91.05416, 105.06981, 117.06976, 191.08542, 84.08073, 155.08545, 218.10875, 205.10098, 58.06533, 179.08548, 129.06972	0.62	2.28	0.51	2.04	1.27	1.16	7.790
M1, NOR	$C_{19}H_{21}N$	264.17468	233.13228, 91.05417, 105.06982, 117.06978, 264.17407, 191.08539, 155.08543, 218.10884, 205.101, 70.06513, 179.08543, 129.06966	1.02	0.55	-0.14	1.36	0.90	1.13	7.608
M2	$C_{20}H_{23}NO$	294.18528	276.17438, 231.11673, 58.06536, 216.09325, 84.08076, 191.08553, 205.10109, 294.18396, 233.13249, 117.06985, 229.10129, 203.08531, 249.12743	1.03	2.59	0.62	1.66	0.83	0.93	4.693
M3	$C_{20}H_{23}NO$	294.18528	276.17297, 231.11662, 58.06536, 216.09288, 191.08527, 84.0808, 193.10109, 205.10126, 233.13242, 294.20566, 117.07016	0.20	1.86	1.55	1.35	1.03	0.83	5.554
M4	$C_{19}H_{21}NO$	280.16958	231.11665, 262.15875, 216.0932, 191.08545, 70.06516, 205.10114, 229.10118, 153.06975, 115.05423, 215.08548, 203.08553	0.45	0.78	0.23	1.76	1.43	1.31	4.550
M5	$C_{19}H_{21}NO$	280.16958	231.11676, 262.15884, 216.09328, 191.08549, 70.06519, 205.10123, 193.10095, 153.06979, 229.101, 115.05428, 215.08527	0.45	1.00	1.54	1.32	-	1.11	5.392
M6	$C_{20}H_{23}NO$	294.18528	276.17413, 231.11673, 58.06536, 180.17464, 98.09641, 216.09317, 84.08082, 294.18256, 191.08546, 205.10118, 249.12727	-	-	-0.11	-	-	-	4.615

Compound	Molecular Formula (M)	Theoretical m/z ($[M+H]^+$)	Fragments in MS2 spectra	ΔMass (ppm)						R_t (min)
				Liver	Plasma	Bile	Brain	Muscle	Gill	
M7	$C_{20}H_{23}NO$	294.18528	233.13234, 91.05421, 105.06988, 117.06982, 191.08546, 155.08553, 218.10884, 205.1011, 58.06531, 179.08623, 129.07007	0.83	1.45	0.00	-	-	0.72	8.125
M8	$C_{20}H_{21}N$	276.17468	276.17407, 231.11671, 58.06536, 216.09323, 84.08077, 205.10114, 191.08545, 229.1013, 117.06993, 233.13214, 203.08549, 91.05421, 98.09637	1.52	2.08	-	-	-	1.19	4.694
M9	$C_{19}H_{19}N$	262.15898	231.1167, 262.15845, 216.09325, 191.08548, 70.06516, 205.10109, 229.10103, 153.06992, 215.08545, 115.05424, 203.08536	0.70	-	-	-	-	1.39	4.549
M10	$C_{20}H_{21}NO$	292.16958	84.08076, 292.16882, 229.10103, 219.11673, 58.06536, 247.11159, 91.0542, 274.15845, 203.08537, 178.07761, 191.08534, 68.04969, 72.08083	0.96	3.25	-	1.79	0.85	0.54	5.767
M11	$C_{20}H_{21}NO$	292.16958	84.0808, 292.16937, 229.10115, 219.11679, 58.06538, 247.11156, 91.05424, 274.15872, 178.07773, 203.08549, 191.08556	-	1.27	1.16	-	-	-	6.039
M12	$C_{20}H_{21}NO$	292.16958	229.10101, 260.14304, 203.08533, 232.11188, 70.06513, 292.16919, 82.06504, 231.11691, 292.22525, 179.08549	0.43	-	0.43	1.48	1.37	1.48	7.743
M13	$C_{21}H_{23}NO$	306.18528	274.15848, 84.0807, 229.10088, 203.08524, 58.06531, 231.11652, 306.18451, 261.12689, 216.09306, 96.08065	0.50	1.29	0.00	0.99	-2.11	0.99	7.943
M14	$C_{19}H_{19}NO$	278.15398	229.10095, 247.11147, 70.06513, 219.11656, 91.05416, 278.15338, 219.08002, 260.14307, 203.08533, 178.07751, 191.08539	0.47	1.90	1.02	0.80	0.25	0.91	5.627
M15	$C_{20}H_{23}NO_2$	310.18018	231.11664, 216.09315, 58.06535, 191.08571, 229.10075, 219.11623, 292.16919, 115.0543, 153.06981, 178.07756, 91.05417, 84.08066, 249.12926	1.61	0.52	0.43	-	-	-	4.915

Compound	Molecular Formula (M)	Theoretical m/z ($[M+H]^+$)	Fragments in MS2 spectra	ΔMass (ppm)						R_t (min)
				Liver	Plasma	Bile	Brain	Muscle	Gill	
M16	$C_{20}H_{23}NO_2$	310.18018	231.11639, 216.09314, 58.06528, 191.08519, 219.11652, 229.10063, 292.16824, 91.0541, 178.07793, 203.08435, 84.08055, 264.17496, 249.12704	-	0.72	0.92	-	-	-	5.977
M17	$C_{20}H_{23}NO_2$	310.18018	219.11667, 264.17441, 191.08542, 178.07756, 292.16922, 91.05419, 58.06536, 84.08076, 310.17923, 247.11148, 229.1011	1.41	0.72	0.23	-	-	1.51	4.228
M18	$C_{20}H_{23}NO_2$	310.18018	219.11673, 264.17441, 310.17804, 191.08545, 58.06538, 292.1651, 178.07745, 91.05416, 84.08081, 229.10124, 247.11192	1.61	0.82	1.02	-	-	1.41	3.320
M19	$C_{20}H_{23}NO_2$	310.18018	292.16925, 247.11156, 58.06537, 219.11667, 310.17978, 264.17444, 84.08076, 221.09608, 229.101, 207.08025, 232.08778	-	-	0.62	-	-	-	3.288
M20	$C_{19}H_{21}NO_2$	296.16448	219.11659, 191.08542, 250.15869, 178.07761, 193.10109, 91.05418, 70.06512, 229.10104, 247.11111, 278.15268, 260.14301	0.98	-	-1.08	-	-	1.50	4.155
M21	$C_{19}H_{21}NO_2$	296.16448	219.11662, 250.15906, 191.08537, 178.07759, 91.05424, 193.10124, 264.20703, 247.1116, 296.23312, 70.06517, 229.10097, 278.15073	1.91	-	-	-	-	-	3.204
M22	$C_{20}H_{21}NO_2$	308.16448	229.10095, 219.11658, 91.05418, 58.06534, 247.11148, 217.10104, 178.07762, 191.08537, 207.08023, 308.16293, 84.08074, 290.15366	-	1.44	0.35	-	-	-	6.153
M23	$C_{18}H_{20}O_2$	269.15358	116.10699, 58.06538, 137.04582, 154.05327, 99.08046, 228.23216, 211.11049	3.33	-	-	-	-	-	0.722
M24	$C_{26}H_{31}NO_8$	470.21738	276.17426, 231.11665, 58.06534, 294.18494, 216.0932, 84.08076, 191.08548, 205.10101, 203.08492, 117.06969, 249.12755	0.55	-	1.26	-	-	-	3.896

Compound	Molecular Formula (M)	Theoretical m/z ($[M+H]^+$)	Fragments in MS2 spectra	ΔMass (ppm)						R_t (min)
				Liver	Plasma	Bile	Brain	Muscle	Gill	
M25	$C_{26}H_{31}NO_7$	470.21738	276.17432, 231.1167, 58.06536, 294.18491, 216.09311, 191.08546, 84.08077, 205.10109, 249.12769, 117.06975, 203.08606	-	0.16	0.81	-	-	-	3.945
M26	$C_{26}H_{31}NO_7$	470.21738	276.17419, 231.11671, 58.06537, 294.18497, 216.09315, 84.08077, 191.08531, 205.10147, 249.12872, 203.08517, 117.06951	0.48	-0.10	0.87	-	-	-	3.736
M27	$C_{26}H_{31}NO_7$	470.21738	231.11671, 262.15875, 216.09323, 191.08548, 70.06514, 276.17444, 205.1011, 229.10123, 153.06984, 115.05424, 294.18439	-	-	0.09	-	-	-	4.642
M28	$C_{26}H_{31}NO_7$	470.21738	231.11673, 262.15878, 216.09325, 191.08543, 70.06518, 205.1011, 153.06979, 229.1015, 115.05432, 276.17566, 203.08513	-	-	-0.69	-	-	-	5.025
M29	$C_{26}H_{31}NO_7$	470.21738	294.18494, 249.12721, 470.21844, 105.06985, 155.08554, 84.08077	-	-	-0.69	-	-	-	3.481
M30	$C_{26}H_{31}NO_8$	486.21228	292.16928, 247.11157, 58.06538, 310.17987, 468.20126, 207.08031, 84.08077, 219.11812	-	-	-0.20	-	-	-	2.222
M31	$C_{26}H_{31}NO_8$	486.21228	231.11681, 250.15892, 219.11676, 58.06541, 191.08559, 216.09349, 278.15396, 310.18048, 292.16974, 178.07774	-	-	-0.83	-	-	-	4.224
M32	$C_{25}H_{29}NO_7$	456.20168	262.15878, 231.1167, 216.09329, 191.08549, 70.06517, 205.10101, 153.07027, 219.11626, 115.05406	-	-	0.04	-	-	-	3.905
M33	$C_{25}H_{29}NO_7$	456.20168	262.15881, 231.11676, 216.09331, 191.08563, 70.0652, 205.10117, 153.06975, 219.11646, 115.05421	-	-	0.31	-	-	-	3.771

(-): not detected

Metabolite Identification

- **M1, Nortriptyline (NOR): N-demethylation**. M1 was identified N-demethylation of AMI, which is commonly known as nortriptyline (NOR), and we confirmed the structure using a reference standard due to the same mass, retention time and MS2 spectra (see Table S2). The identification of M1 was performed according to the following fragments with m/z 233, 218, 205, 191, 179, 155, 129, 115, 117, 105, 91 and 70. While the fragment m/z 70 pinpoints that the side chain contains one methyl group less than AMI ($[84 - CH_2]^+$) and the absence of m/z 58 indicates that the amine head group has been modified, the rest of the fragments were identical to AMI (see AMI fragmentation in Figure 3).
- **M2-M3: monohydroxylated metabolites of AMI in the ethylene group of the central ring.** The annotation was performed according to the following fragments (see Figure S1a): *m/z* 276 ($[294 - H_2O]^+$), 249 ($[294 - C_2H_7N]^+$), 231 ($[AMI - C_2H_7N\text{-}H_2]^+$), 216 ($[AMI - C_3H_{10}N\text{-}H_2]^+$), 203 ($[AMI - C_4H_{11}N\text{-}H_2]^+$) and 84 ($[C_5H_{10}N]^+$). Actually, while fragments m/z 276, 249 and 231 could indicate hydroxylation at either the endo- or exo- ethylene group of AMI, fragments 216 (218-2) and 203 (205-2) are only possible if hydroxylation occurred at the central ring. Furthermore, the fragment m/z 84 indicates that the side chain remains intact compared to AMI (see Figure 3 for AMI fragmentation). Fragment ion *m/z* 249 ($[294 - C_2H_7N]^+$) suggests that the hydroxylation occurs in the three-carbon area between the nitrogen atom and the central ring. However, we disagree with that statement since fragment *m/z* 249 corresponds to the oxidation of fragment *m/z* 233 present in AMI (*m/z* 233+16=249), independently of whether the oxidation occurs in the central ring or in the side chain of the molecule.
- **M4-M5: monohydroxylation of NOR in the ethylene group of the central ring.** Both metabolites showed a similar fragmentation pattern, suggesting that hydroxylation had occurred in the central ring, due to the presence of the fragment ions m/z 262 (loss of water) and fragments 231 ($233\text{-}H_2$) and 216 ($218\text{-}H_2$), indicative of loss of water occurring at the endocyclic ethylene group. The presence of unmodified m/z 70 ($[C_4H_6N]^+$) also pinpoints that the hydroxylation of NOR occurred in the ethylene group of the central ring.
- **M6: monohydroxylated metabolite of AMI in the ethylene group of the side chain.** Compared with the fragmentation observed for M2-M3, the presence of the fragment at m/z 98 should be highlighted (see Figure S1). While fragments m/z 276, 249 and 231 pinpointed once again hydroxylation at either the endocyclic or the exocyclic ethylene

groups, the fragment m/z 98 ($[C_6H_{14}N]^+$) was indicative of a modification in the side chain that induced the loss of $[C_6H_{14}N]^+$ (see Figure S1b). Although fragments m/z 216 ($[AMI - C_3H_{10}N\text{-}H_2O]^+$) and m/z 84 ($[C_5H_{10}N]^+$) were also present, the higher intensity of m/z 98 was prioritized.

- **M7: N-oxidation of AMI.** M7 metabolite was annotated as a *N*-oxidation of AMI (commonly known as amitriptylinoxide) due to the absence of a loss of water during fragmentation and unmodified AMI skeleton with the presence of fragment ions m/z 233 and 218, also present in AMI (see Figure 3 for AMI fragmentation). We presume M7 corresponds to a N-oxidation and not to the oxidation of a N-methyl group due to the presence of the unmodified tertiary amine head with fragment m/z 58 ($[C_3H_8N]^+$) and the absence of fragment m/z 264 ($[AMI+O\text{-}CH_2O]^+$).
- **M8: Dehydration of M2-M3.** M8 metabolite corresponds most probably to the dehydratation of M2-M3 according to the similar fragmentation pattern observed. The presence of fragment ions m/z 276 ($[278\text{-}H_2]^+$), 231 ($[233\text{-}H_2]^+$) and 216 ($[218\text{-}H_2]^+$) pinpoint a dehydrogenation of AMI. While fragments m/z 276 and 231 could indicate a dehydrogenation at either the endocyclic or exocyclic ethylene groups, the fragment at m/z 216 could only be explained if the dehydrogenation occurred at the ethylene group of the central ring. Fragment m/z 98, which could pinpoint a dehydrogenation in the ethylene group of the side chain, was also present but since the intensity of this peak was much smaller than the signal for m/z 216 and m/z 84 fragments, we concluded that dehydrogenation had occurred at the central ring.
- **M9: Dehydration of M4-M5.** Similarly to M8, M9 corresponds most probably to the dehydratation of M4-M5 according to the similar fragmentation pattern observed. The presence of fragment ions m/z 262 ($[264\text{-}H_2]^+$, 231 ($[233\text{-}H_2]^+$) and 216 ($[218\text{-}H_2]^+$) pinpoint a dehydrogenation of NOR. In addition, due to the presence of the fragment m/z 70, we could conclude that the side chain of NOR remains intact, and therefore, dehydrogenation had occurred at the central ring.
- **M10-M11: keto-derivatives of AMI in the central ring**. The small signal observed for the fragment m/z 274, corresponding to a loss of water ($[292\text{-}H_2O]^+$), could be attributed to the enolic form of the keto group (see Figure S2a for fragmentation). Similarly, fragments m/z 247 ($233+O\text{-}H_2]^+$), 229 ($[233\text{-}H_2\text{-}H_2]^+$) and 219 ($[233\text{-}CH_2]^+$) also pinpointed an oxygenation combined with a dehydrogenation but were not indicative of the position of the keto group, which could be located either in the exocyclic or endocyclic ethylene groups. However, the high intensity of fragments 84 and 58

(indicative of an unmodified side chain of AMI) suggested that the keto group was located at the central ring.

- **M12: Dehydrogenation plus methoxylation of NOR.** Compared to the fragmentation of M10-M11, the lack of loss of water, the lack of fragments m/z 84 ($[C_5H_{10}N]^+$) and m/z 58 ($[C_3H_8N]^+$), and the presence of fragments m/z 260 ($[C_{19}H_{18}N]^+$), m/z 203 ($[C_{16}H_{11}N]^+$), m/z 82 ($[C_5H_8N]^+$) and m/z 70 ($[C_4H_8N]^+$) (see Figures S2a and S2b) could indicate a dehydrogenation in the ethylene group and a loss of methanol group. Fragment ion m/z 203 ($[205\text{-}H_2]^+$) is indicative of a dehydrogenation occurring in the endocyclic ethylene group of the central ring and, this, together with no fragment indicating the presence of an oxygenation in the rings, pinpoints that the dehydrogenation observed in M12 should be in the central ring. Besides, fragment m/z 70 is a typical fragment in NOR fragmentation. This fact, together with the presence of fragment m/z 260 related with a loss of CH_3OH suggests the presence of a methoxy group in the exocyclic ethylene group. However, we cannot explain the presence of fragments m/z 82 ($[C_5H_8N]^+$) and 232.
- **M13: Dehydrogenation plus methoxylation of AMI.** M13, with an exact mass of 306.1857 ($C_{21}H_{23}NO$), showed a similar structure to M12 but with the tertiary amine head as in AMI (m/z 58), with characteristic fragment ions (see Figure S2c) m/z 274 ($306\text{-}[CH_3OH]^+$), m/z 229 and m/z 203 ($[205\text{-}H_2]^+$). The latter suggests the presence of a double bond in the endocyclic ethylene group of the central ring. However, we cannot explain fragment m/z 84.
- **M14: Epoxy metabolite of M9**. M14, with an exact mass of 278.2544 showed the presence of fragments m/z 260 ($278\text{-}[H_2O]^+$), m/z 247, m/z 219, m/z 203 and the unmodified side chain (m/z 70) pinpointed that M14 corresponded to an epoxy metabolite of NOR.
- **M15-M16: Hydroxylation in the ethylene group of the central ring and N-oxidation of AMI.** M15 and M16 showed a similar fragmentation pattern, with a single loss of water (m/z 292) and with the presence of fragments m/z 249, m/z 231, m/z 216, m/z 84 and m/z 58. Fragment ions m/z 249 and 231 and the loss of water indicate that one of the hydroxylations occurs in an ethylene group, while fragment 216 pinpoints that it corresponds to the central ring. Regarding the second hydroxylation, the presence of fragment ions m/z 231 and m/z 216 is incompatible with aromatic hydroxylation, and hence, the second hydroxyl group should be located at the tertiary amine of AMI.

Since m/z 84 and 58 were observed, no modification is presumed, and therefore we suggest a *N*-oxidation.

- **M17-M19: dihydroxy-metabolites of AMI in the ethylene group of the central ring**. M17-M19 metabolites with m/z 310.1807 were annotated as dihydroxy-metabolites in the ethylene group of the central ring (see Figure S3a) according to the presence of the fragments m/z 292 ($[310\text{-}H_2O]^+$), m/z 247 ($[233\text{+}O\text{-}H_2]^+$), m/z 264 ($[C_{19}H_{22}N]^+$), m/z 219 ($[C_{17}H_{15}N]^+$), m/z 84 ($[C_5H_{10}N]^+$) and m/z 58 ($[C_3H_8N]^+$). The presence of a loss of water (m/z 292) and the unmodified side chain (m/z 84 and m/z 58) suggest the presence of a hydroxyl group in the ethylene group of the central ring. For the location of the second hydroxyl group, fragments m/z 264 ($[AMI\text{-}CH_2]^+$) and 219 ($[233\text{-}CH_2]^+$) could be highlighted, which correspond to the demethylation of AMI structure at the central ring caused after cleavage of the central ring (see Figure S3a). The reason of not detecting a second loss of water could be the low intensity of the fragment formed after this second loss of water in the central ring, which gives rise to a low stability triple bond. Therefore, we concluded that the second hydroxyl group was also present in the endocyclic ethylene of the central ring.
- **M20-M21: dihydroxy-metabolites of NOR in the ethylene group of the central ring**. In the case of M20 (see Figure S3b) with m/z 296.1650, similar as for M17-M19, it was suggested that both hydroxy groups were located in the ethylene group of the central ring, taking into account the following characteristic fragments: m/z 278 ($[296\text{-}H_2O]^+$), m/z 260 ($[278\text{-}H_2O]^+$), m/z 247 ($[233\text{+}OH\text{-}H_2]^+$), m/z 250 ($[C_{18}H_{20}N]^+ \equiv [M1\text{-}CH_2]^+$), m/z 219 ($[233\text{-}CH_2]^+$) and m/z 70 (unmodified side chain). As the fragment indicating the second loss of water (m/z 260) was very weak in M20, and the fragments m/z 250 and m/z 219 are related with the cleavage of the ethylene group at the central ring, it was suggested that both hydroxy groups were located in the endocyclic ethylene group. M21 showed a similar fragmentation but the second loss of water was not observed, probably due to the lower intensity of the fragments obtained for M21. M21, was therefore, also annotated as a dihydroxymetabolite of NOR in the ethylene group of the central ring.
- **M22: dehydrogenation of M15-M16 or *N*-oxidation of M10-M11.** M22 with m/z 308.1650 was suggested to be N-oxidation of AMI with a keto group in the central ring. It is characterised by the presence of only a small signal for fragment m/z 290, corresponding to a loss of water ($[308\text{-}H_2O]^+$), and a fragmentation pattern similar to that observed for M10-M11.

- **M23. Dihydroxylation of AMI or NOR without the dimethylenamine or methylenamine group.** Either AMI or NOR lost the C_2H_6N or the CH_3N group and a dihydroxylation occurred. However, due to the poor fragmentation observed we could not locate these two hydroxyl groups.
- **M24, M25, M26: glucuronides of M2-M3.** Once the loss of the glucuronide group (-176 Da) occurred, the fragmentation pattern observed was similar to M2-M3. We could not determine where the conjugation (*N*- or *O*-glucuronidation) occurred.
- **M27-M28. N-glucuronides of a methoxy metabolite of NOR.** With an exact mass of m/z 470.2178 (see Figure S4 for fragmentation) M27-M28 showed fragment ions m/z 276 (low abundance) and m/z 216, which suggest the presence of a hydroxyl group at the ethylene group of the central ring. However, the presence of an oxidation at that position does not explain the high abundances obtained for fragment ions m/z 262 and m/z 70. We could only explain the presence of m/z 70 (typical fragment in NOR) and m/z 262 if M27-M28, were not considered as glucuronides of AMI but N-glucuronides of methoxy-metabolite of NOR in the ethylene group of the central ring. The loss of the methoxy group could explain the high intensity of fragment ion m/z 262 (294-$[CH_3OH]^+$).
- **M29: Glucuronide of a hydroxyl metabolite of AMI in an aromatic ring.** Although monohydroxy-metabolites of AMI in the aromatic ring were not observed in the present work, M29 was attributed to a glucuronide of a hydroxyl metabolite of AMI in an aromatic ring due the lack of loss of water and the presence of fragment *m/z* 249 ($[233+O]^+$).
- **M30: Glucuronide of M17-M19**. With an exact mass of 486.2127, M30 was attributed to the glucuronidation of M17-M19 due to the presence of fragment ions m/z 292 (loss of water) and m/z 247 ($[231+O]^+$).
- **M31**: **not elucidated.** In the case of M31 we could not define the structure of this glucuronide metabolite. Although fragments m/z 292 and m/z 216 could suggest that one of the hydroxyl groups was located at the ethylene group of the central ring, we could not explain the presence of fragments m/z 250 and 278. The latter could be better explained if the glucuronide belonged to a methoxy-metabolite of NOR.
- **M32-M33: Glucuronides of M4-M5.** Glucuronides M32-M33 showed a similar fragmentation in accordance with the fragmentation of M4-M5 monohydroxylates of NOR.

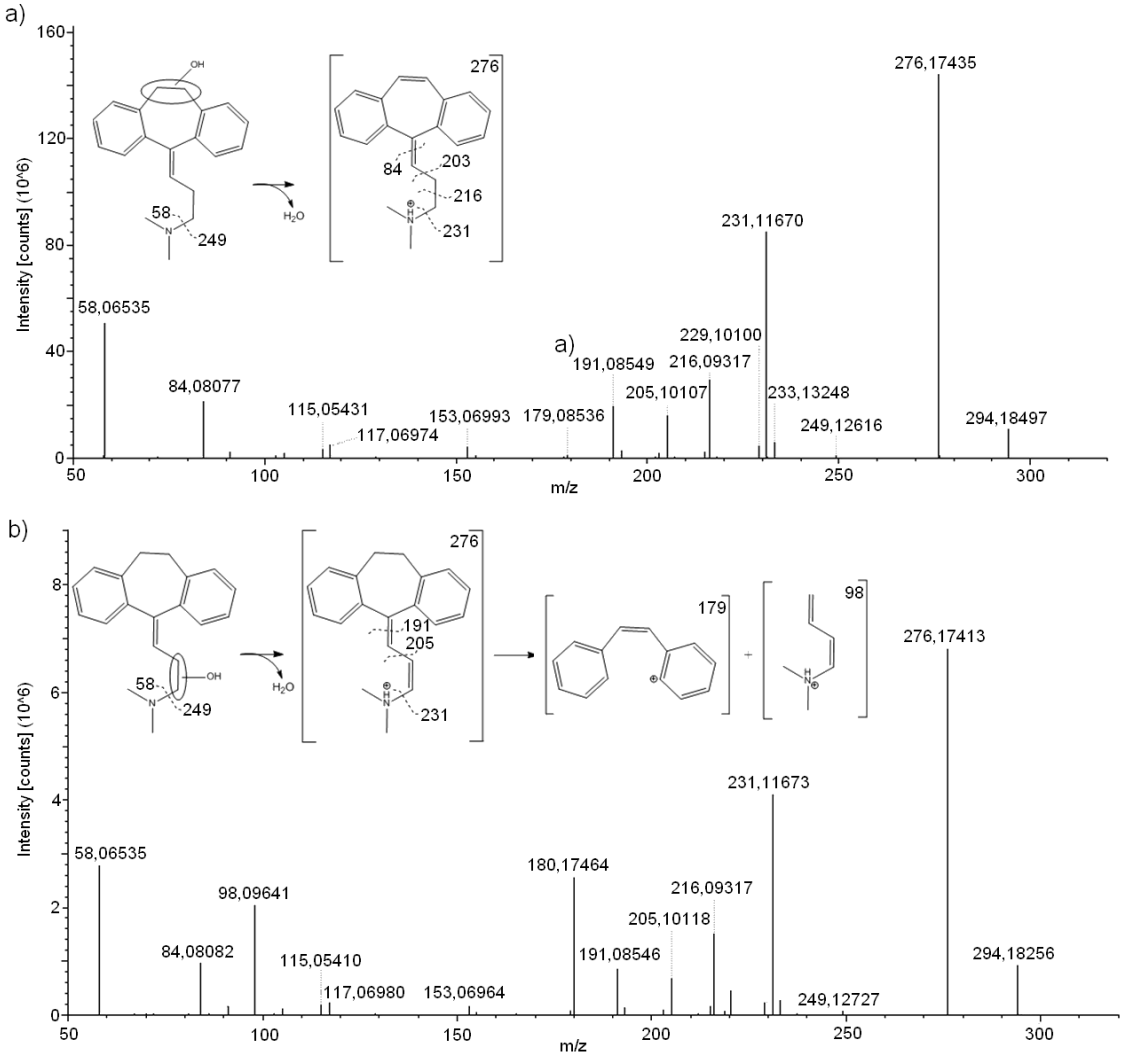

Figure S1: MS2 spectra and fragmentation of a) M2-M3, and b) M6

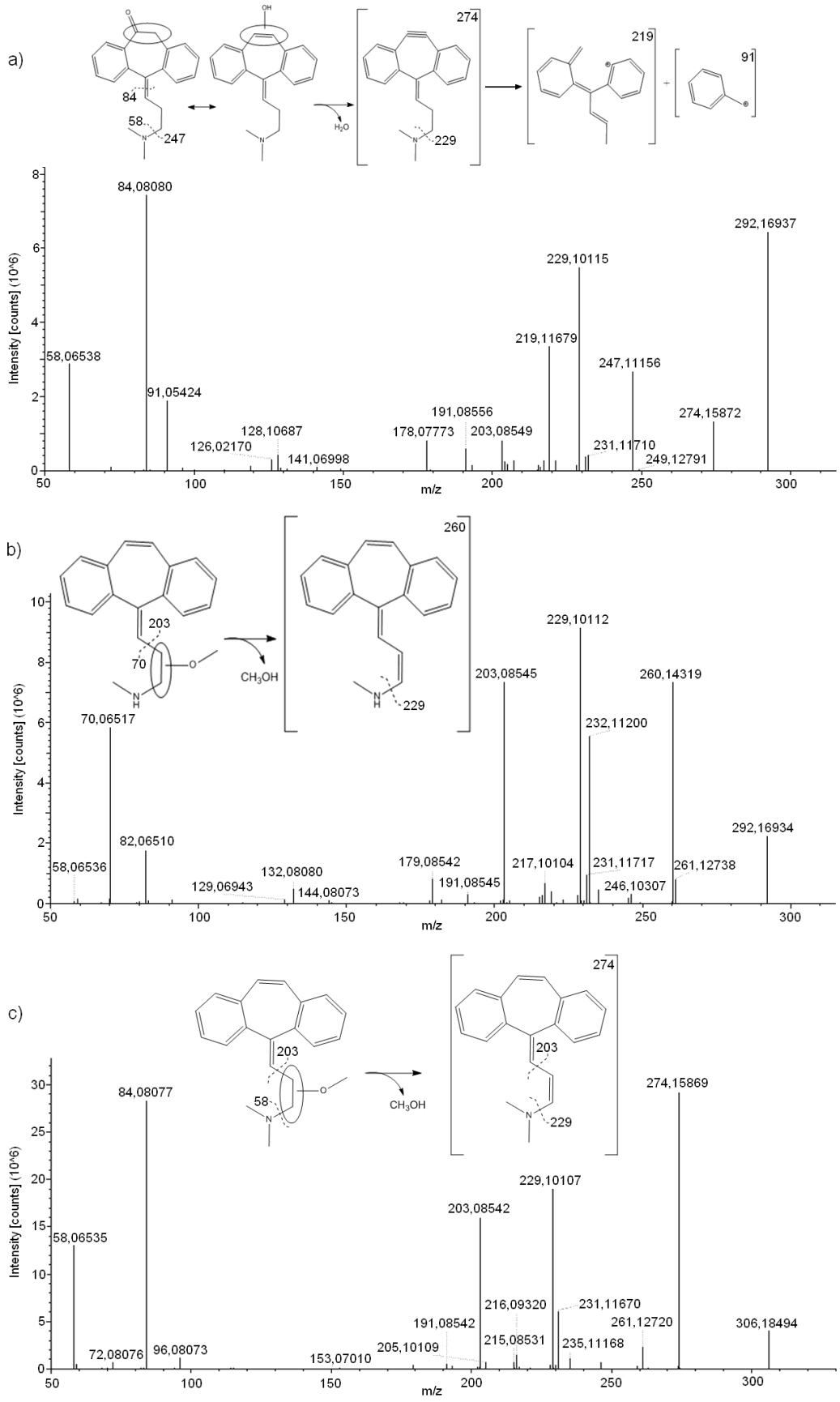

Figure S2: MS2 spectra and fragmentation of a) M10-M11, b) M12, and c) M13

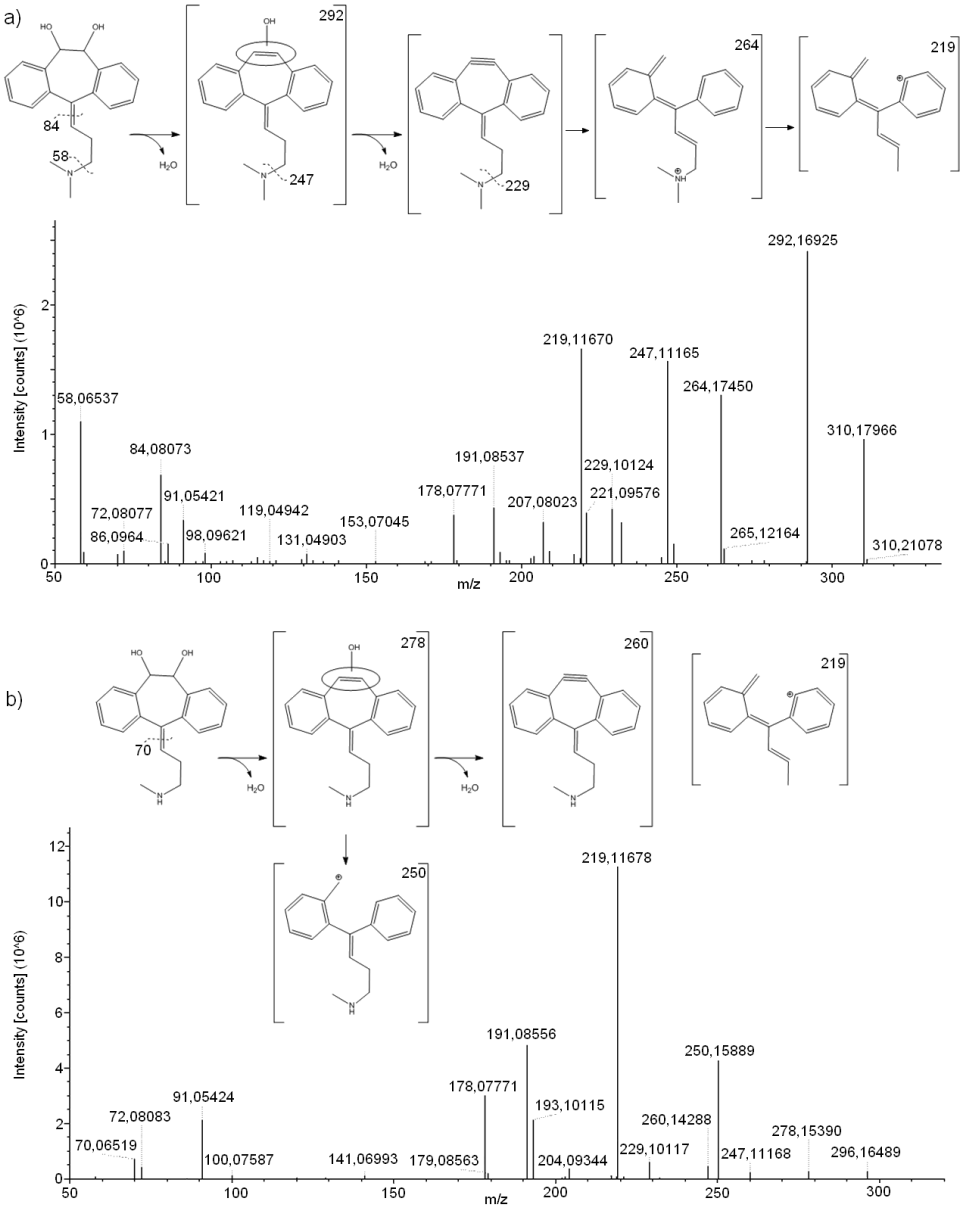

Figure S3: MS2 spectra and fragmentation of a) M17-M18-M19, and b) M20

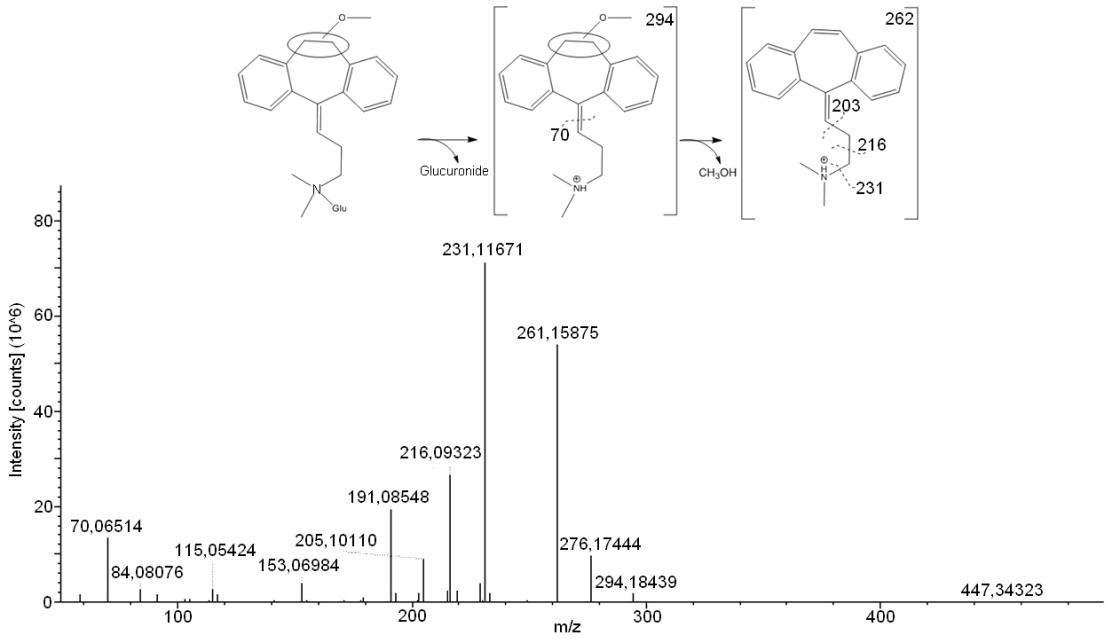

Figure S4: MS2 spectra and fragmentation of M27-M28